NMRF / RR / 03 /2015

RESEARCH REPORT

Verification of Met Office Unified Model (UM) quantitative precipitation forecasts during the Indian monsoon using the Contiguous Rain Areas (CRA) method

Raghavendra Ashrit, Elizabeth Ebert*, Ashis K. Mitra, Kuldeep Sharma, G. R. Iyengar and E. N. Rajagopal

March 2015

National Centre for Medium Range Weather Forecasting
Ministry of Earth Sciences, Government of India
A-50, Sector-62, NOIDA, India 201 309

Verification of Met Office Unified Model (UM) quantitative precipitation forecasts during the Indian Monsoon using the Contiguous Rain Area (CRA) method

Raghavendra Ashrit, Elizabeth Ebert*, Ashis K. Mitra, Kuldeep Sharma, Gopal Iyengar and E.N. Rajagopal

National Centre for Medium Range Weather Forecasting
Noida, India

***Centre for Australian Weather and Climate Research**
Melbourne, Australia

National Centre for Medium Range Weather Forecasting
Ministry of Earth Sciences
A-50, Sector 62, NOIDA-201309, INDIA

March 2015

Earth System Science Organisation
National Centre For Medium Range Weather Forecasting Document Control Data Sheet

1	Name of the Institute	National Centre for Medium Range Weather Forecasting
2	Document Number	*NMRF/RR/03/2015*
3	Date of publication	March 2015
4	Title of the document	Verification of Met Office Unified Model (UM) quantitative precipitation forecasts during the Indian Monsoon using the Contiguous Rain Area (CRA) method
5	Type of Document	Research Report
6	No.of pages & Figures	32 Pages, 15 Figures and 3 Tables
7	Number of References	31
8	Author (S)	Raghavendra Ashrit, Elizabeth Ebert*, Ashis K. Mitra, Kuldeep Sharma, Gopal Iyengar and E.N. Rajagopal
9	Originating Unit	NCMRWF
10	Abstract (100 words)	The operational medium range rainfall forecasts of the Met Office Unified Model (UM) are evaluated over India during six monsoon (JJAS) seasons from 2007-2012 using the Contiguous Rainfall Area (CRA). The forecasts show a wet bias (due to excessive number of rainy days) and higher rainfall frequency for thresholds of 0-20 mm d^{-1}. Over the South-West (SW) India, the forecasts tend to underestimate rain intensity and the events tended to be displaced to the west and southwest of the observed position on an average by about 1° distance. Over eastern India (E) forecasts of lighter (*heavy*) rainfall events tend to be displaced to the east on an average by about 1°(*southwest by 1-2 9*). In all four regions, the relative contribution to total error due to displacement increases with increasing CRA threshold.
11	Security classification	Non-Secure
12	Distribution	Unrestricted Distribution
13	Key Words	

Abstract

The operational medium range rainfall forecasts of the Met Office Unified Model (UM) are evaluated over India using the Contiguous Rainfall Area (CRA) verification technique. In the CRA method, forecast and observed weather systems are objectively matched to estimate location, volume, and pattern errors. Daily rainfall forecasts from six (2007-2012) monsoon seasons are verified against two observed rainfall datasets, the Tropical Rainfall Measuring Mission (TRMM) rainfall and the India Meteorological Department and NCMRWF merged rainfall data (NSGM).

The model forecasts show a wet bias (due to excessive number of rainy days) and higher rainfall frequency for thresholds of 0-20 mm d^{-1} when verified against both observed data sets. Verification against the NSGM data consistently suggests higher skill in the forecasts as compared to TRMM data. Forecast rain systems are also verified using 10, 20 and 40 mm d^{-1} CRA thresholds for four sub-regions namely (a) north west (NW) (ii) south west (SW) (iii) eastern (E) and (d) north east (NE) sub-region. Over the SW sub-region, the forecasts tend to underestimate rain intensity. In the SW region, the forecast events tended to be displaced to the west and southwest of the observed position on an average by about 1° distance. Over eastern India (E) forecasts of lighter (*heavy*) rainfall events tend to be displaced to the east on an average by about 1°(*southwest by 1-2°)*. In all four regions, the relative contribution to total error due to displacement increases with increasing CRA threshold. These findings can be useful for forecasters and for model developers with regard to the model systematic errors associated with the monsoon rainfall over different parts of India.

1. Introduction

The rainfall during the monsoon (June-September, JJAS) season contributes over 75% of the annual rainfall in most parts of the Indian subcontinent and is the lifeline for agriculture and economy of the entire region. Forecasting of seasonal rainfall gets great attention due to ensuing drought (flood) conditions. The monsoon rainfall occurs in many sporadic weather events having spatial scales from 100 to 1000 km. The daily and weekly rainfall during the season poses a significant forecasting challenge in Numerical Weather Prediction (NWP). This is due to complex interactions involving topography, treatment of synoptic scale systems, and mesoscale convective systems and non-availability of good quality high resolution observations over land and neighbouring seas.

Numerical weather prediction (NWP) models have undergone significant improvements in the last two decades and have demonstrated reasonable success and skill in short to medium-range weather forecasting (Kalnay et al. 1998; Simmons and Hollingsworth 2002; Harper et al. 2007). However, the predictability of Indian summer monsoon conditions is quite low (Goswami and Ajay Mohan 2001). Drivers of the intraseasonal variability such as the Madden-Julian oscillation modulate the frequency of occurrence of synoptic events such as lows, depressions and tropical cyclones (Maloney and Hartmann 2000; Goswami et al. 2003; Bessafi and Wheeler 2006). Accurate quantitative precipitation forecasting (QPF) still remains a challenge, as evidenced by the frequent

large errors in the predicted precipitation amounts and distribution from NWP models. Factors contributing to these errors include: errors in the initial conditions, predicted flow (dynamics), large-scale and convective rain processes (physics), grid resolution and representation of local land surface characteristics. As a result, the QPFs often have large errors in predicted position of the rain system, shape and size of the rain pattern, and magnitude or intensity of rainfall.

With the enhanced computing capability in recent years, the spatial and temporal resolution of models has also increased. Verification of high resolution forecasts using traditional metrics often suggests poor forecast skill due to the lack of exact matches among the forecast/observation pairs. Several new diagnostic spatial verification approaches have been developed recently that better reflect the quality of the forecasts. Feature-based methods and neighbourhood verification approaches assess the broader forecast quality without over-penalizing the errors at grid scale. Ebert (2008), Ebert and Gallus (2009), and Gilleland et al. (2010) provide a detailed review and intercomparison of several spatial verification methods. The Contiguous Rain Area (CRA) method is a feature-based approach that isolates systems or features of interest and evaluates their properties, namely, location, size, intensity, and pattern. It was one of the first methods to measure errors in predicted location and to separate the total error into components due to location, volume, and pattern errors (Ebert and McBride 2000; Ebert and Gallus 2009).

The present study forms an important component of India's National Monsoon Mission (NMM) Programme to investigate and quantify the rainfall forecast biases in the Unified Model as part of an overall scientific challenge to better predict the Indian monsoon.The medium range rainfall forecasts over India are evaluated in this study to assess the model performance during the monsoon season. The Met Office Unified Model rainfall forecasts (UM hereafter) during the six monsoon (JJAS) seasons from 2007 to 2012 are evaluated using traditional and CRA verification techniques.

There have been quite a few studies reporting rainfall forecast verification over India based on different models (Mandal et al. 2007, Das et al. 2008, Ashrit and Mohandas 2010, Chakraborty 2010, Iyengar et al. 2011). In general these studies indicate that the average root mean squared error (RMSE) of daily rainfall is high (*low*) in higher (*lower*) rainfall regions and that RMSE increases with lead time. Spatial distributions of various performance metrics over Indian land regions show that models tend to have better forecast skill over northern and north-western India (Iyengar et al. 2011). The detailed verification of the UM forecasts and its comparison with National Centre for Medium Range Weather Forecasting (NCMRWF) operational forecasts highlighting the biases are reported in a series of monsoon reports (Iyengar et al, 2011, 2014). This study represents the first application of a diagnostic spatial verification method to rainfall forecasts over India. The data and verification methodology are described in Section 2. Section 3 gives

examples of CRA method applied to rain systems over India and discusses the results in the context of regional performance. The summary and conclusions are given in Section 4.

2. Data and Methodology

2.1 Observed Rainfall Data over India

Figure 1 shows the geographical domain chosen for the present study, 7°-38.5°N, 67°-100.5°E, with the distribution of rain gauges in the India Meteorological Department (IMD) network during the monsoon. Rainfall analyses based on quality controlled observations are critical for verification of the NWP forecasts. In this study we use two observation data sets, (a) the Tropical Rainfall Measuring Mission (TRMM) 3B42 (V7) daily multi-sensor 0.25° x 0.25° gridded rainfall and (b) the IMD and NCMRWF satellite+gauge merged (NSGM) rainfall data at 1°. The TRMM daily rainfall data accumulated at 0000 UTC is used in this study to match with the Met Office forecast which is also accumulated at 0000 UTC. However, the NSGM data which uses 24 hour gauge rainfall and the 3 hourly TRMM estimates is accumulated at 0300 UTC.

TRMM rainfall data have been used in numerous studies since its launch in 1997. TRMM's 3B42 multi-sensor precipitation estimates over the monsoon region are very useful for monsoon studies and verification of rainfall forecasts, since they cover large data sparse oceanic regions. However there are biases over the land regions which require correction (Mitra et al. 2009; Chen et al. 2013). The NSGM objectively analyses IMD

daily rain gauge observations onto a 1° grid using a successive corrections technique with the TRMM 3B42 satellite precipitation providing the first guess field, thus providing spatially continuous rainfall over land and ocean. As noted by Mitra et al. (2009), the 1° grid resolution is appropriate for capturing the large scale rain features associated with the monsoon. The merging of the IMD gauge data into TRMM 3B42 not only corrects the mean biases in the satellite estimates but also improves the large-scale spatial patterns in the satellite field, which is affected by temporal sampling errors (Mitra et al. 2009).

Both the rainfall analyses (TRMM and NSGM) are used in the present study. The higher resolution of the TRMM data may detect spatial detail and heavier rainfall that is not resolved by the coarser NSGM, as can be seen in Figure 2 for the case of 24 hour accumulated rainfall valid for 00Z22nd August 2012. On the other hand, the TRMM estimates sometimes miss out on some of the heavy rain over land that is captured by the gauge observations in the NSGM analysis (Mitra et al. 2009 and Prakash et al. 2014).

A comparison of the frequency of occurrence of rainfall exceeding different thresholds (1, 10, 20, 40, 80, and 160 mm d^{-1}) is shown for both TRMM and NSGM in Figure 3, based on data exclusively over the land regions. While both data sets have similar rain intensity distributions, compared to NSGM, TRMM captures fewer 1 mm d^{-1} rainfall events but detects a higher frequency of 20 and 40 mm d^{-1} events, which can be attributed to relatively higher grid resolution.

2.2 Model Rainfall Forecasts over India

The Met Office Unified Model (UM) is the numerical modelling system developed and used at the Met Office in the United Kingdom (UK) (Davies et al. 2005). In this 'seamless' prediction system different configurations of the same model are used across all time and space scales, with each configuration designed to best represent the processes which have most influence on the timescale of interest. For example, for accurate climate predictions the use of a coupled ocean model is essential, while for short-range weather forecasting a higher resolution atmospheric model may be more beneficial than running a costly ocean component. It can be run in global and limited area domains and can also be coupled to land surface, ocean models, wave models, chemistry and Earth system components.

This study uses the rainfall forecasts from the Met Office operational medium range global model configuration. The Unified Model (UM) is continually developed, taking advantage of improved understanding of atmospheric processes and steadily increasing supercomputer power. The Met Office upgrades its operational NWP configurations up to four times per year. Some of the important changes during the 2007-2012 study period are tabulated in Table 1. The atmospheric model uses non-hydrostatic dynamics with semi-Lagrangian advection and semi-implicit time stepping. It is a grid point model with the ability to run with a rotated pole and variable horizontal grid. A number of sub-grid scale processes are represented, including convection (Gregory and Rowntree

1990, Gregory and Allen 1991, Grant 2001), boundary layer turbulence (Brown et al., 2007), radiation (Edwards and Slingo 1996), cloud microphysics (Wilson and Bollard 1999) and orographic drag (Webster et al., 2003). The model is initialized using a state of the art global four dimensional variational (4DVAR; Rawlins et al., 2007) data assimilation technique. During 2007-2012, the horizontal and vertical resolution of the global configuration improved from about 40 km and 50 levels in 2007 to about 25 km and 70 levels in 2010.

The verification of rainfall forecasts is carried out at all lead times Day1 (t+0 ->t+24h) through Day5 (t+96h -> t+120h). For brevity, the results are presented for Day1 forecasts. It is found that the results for Day2, Day3, Day4 and Day5 forecasts (not shown) are consistent with those of Day1 forecasts. The model forecast rainfall is accumulated at 0000 UTC. The model grid resolution varies from 40 km to 25 km during 2007-2012 (Table 1).

The model forecast and TRMM rainfall are interpolated to NSGM analysis grids (a common grid resolution of 1° x 1°) to enable the verification of large scale daily monsoon rainfall. In this study we use rainfall data over land only, to focus on model performance over land.

2.3 Forecast Verification Approach

The frequency of rain in the forecasts and observations are compared as a first indication of potential biases in model rainfall predictions. The forecast daily rainfall fields are verified using standard

categorical verification scores frequently employed in evaluating precipitation, Probability of Detection (POD), Success Ratio (SR), Probability of False Detection (POFD), Bias Score or Frequency Bias (BIAS) , Equitable Threat Score (ETS) and Hanssen and Kuipers score (HK Score). Descriptions of these scores can be found in standard references on statistical methods (e.g., Jolliffe and Stephenson (2012) and Wilks (2011)).

This is followed by verification using the CRA method to quantify the systematic errors for rain systems. The CRA method is a feature-based verification procedure suitable for gridded forecasts that was developed for estimating the systematic errors in forecasts of rainfall systems (Ebert and McBride 2000; Ebert and Gallus 2009). In addition to measuring errors in predicted location, the CRA method decomposes the total error into components due to errors in location, volume and pattern. The location errors in the model forecasts suggest issues with the model dynamics. The volume and pattern errors possibly emanate from physics and thermodynamics. The steps involved in the CRA technique are described in Ebert and Gallus (2009). A brief summary of the procedure is given here.

A CRA is defined for an observation/forecast pair based on a user-specified isohyet (rain rate contour) in the forecast and/or the observations. It is the *union* of the forecast and observed rain entities as illustrated in Figure 4. This simple approach is used to match a forecast rain system with an observed rain system under the assumption that they

are associated with a common synoptic situation, which is reasonable for monsoon rain events. During the monsoon season, large parts of India regularly receive rainfall in the range up to 10 mm d^{-1}. It was found that choice of 1, 2, and 5 mm d^{-1} contour frequently spread the CRA across large geographical areas, merging unrelated rain systems. CRAs defined by higher thresholds of 10, 20, 40 and 80 mm d^{-1} were used to better isolate the heavy rain events of interest in this study.

In the next step a pattern matching technique is used for estimating the location error. Here the forecast field is horizontally translated over the observed field until the best match is obtained. The geometric distance between the centres of gravity (COG) in the observed and estimated fields forms the location error or vector displacement. The best match between the two entities can be determined either: (a) by maximizing the correlation coefficient, (b) by minimizing the total squared error, (c) by maximizing the overlap of the two entities, or (d) by overlaying the centres of gravity of the two entities. For a good forecast, all of the methods will give very similar location errors. In the present study, the best match is determined by maximizing the correlation, as was also done by Ebert and Gallus (2009).

The mean squared error (MSE) and its decomposition (location error, volume error and pattern error) are computed as shown below (see Grams et al. 2006, for details of the derivation).

$$MSE_{Total} = MSE_{Displacement} + MSE_{Volume} + MSE_{Pattern} \quad (1)$$

where the component errors are estimated as

$$MSE_{Displacement} = 2\boldsymbol{s_F s_O}\,(r_{OPT} - r),$$

$$MSE_{Volume} = (\boldsymbol{F' - O'}), \qquad (2)$$

$$MSE_{Pattern} = 2\boldsymbol{s_F s_O}\,(1 - r_{OPT}) + (\boldsymbol{s_F - s_O})^2$$

In the above expressions $\boldsymbol{F'}$ and $\boldsymbol{O'}$ are the mean forecast and observed precipitation values after shifting the forecast to obtain the best match, $\boldsymbol{s_F}$ and $\boldsymbol{s_O}$ are the standard deviations of the forecast and observed precipitation, respectively, before shifting. The spatial correlation between the original forecast and observed features (r) increases to an optimum value (r_{OPT}) in the process of correcting the location via pattern matching. The number of 'good matches' corresponds to the number of forecasts that matched well with observations when the optimum correlation (r_{OPT}) was (statistically) significantly greater than zero (accessed via two tailed t-test).

3. Results of Rainfall Forecast Verification

3.1 Evaluation of Forecast Rain Occurrence during 2007-2012

As discussed in the introduction, forecasting of rainfall over India and tropics in general is a challenge for the NWP models. While the models generally capture large scale features of the monsoon rainfall distribution, they fail to reproduce the regional peculiarities. This is evident even in the observed and forecast seasonal mean rainfall over India. The observed and forecast mean JJAS rainfall over India during 2012 is shown in Figure 5 for forecasts with different lead times. The forecasts successfully capture the gross features of mean monsoon

rainfall in terms of high rainfall amounts (16-32 mm d^{-1}) along the west coast and reducing rainfall amounts eastwards over the peninsula. Similarly, the model captures high rainfall amounts (16-32 mm d^{-1}) over northeast India and reducing rainfall amounts westwards over northwest India. The model shows large biases in rainfall over northern India adjoining the Himalayas. This feature is typical and can be seen during each of the monsoon seasons. The low level winds (850 hPa; not shown) over the Gangetic plains typically show strong easterly bias (Iyengar et al. 2011) which partly explains the rainfall bias over that region. To further examine the bias in the rainfall forecast, climatologically frequency is constructed although using the available 7 years of data. The frequency of rainfall occurrence in excess of different thresholds is shown in Figure 6 for the Day1 forecasts and the two observation data sets (TRMM and NSGM). The model overestimates the rainfall frequency at all thresholds below 20 mm d^{-1}. Figure 6 is based on all rainy days in the seven monsoon seasons; this model behaviour was consistently seen in each of them.

It is also found that the model features high number of rainy days compared to observations. This is presented in the form of a spatial distribution of the rainy day counts over India in Figure 7. The panels (a) and (b) show the observed (NSGM) and forecast count of rainy days (rainfall >1mm d^{-1}). The difference between the two is striking with the forecasts having a higher number of rainy days, particularly where the number of rainy days is observed to be lower than average, in nearly all

parts of India. The forecasts have an excessive number of rainy days, throughout the SW, E and NE regions of India. Even over most of the dry region of NW the model predicts a relatively higher number of rainy days. The panels (c) and (d) show the rainy day counts in the UM forecasts with 2mm d^{-1} and 5mm d^{-1} thresholds respectively. The 5mm d^{-1} threshold produces a more realistic pattern overall of the rainy day counts where the number of rainy days is observed to be higher than average. On the other hand, large parts of the peninsula show a reduced number of rainy days particularly where the number of rainy days is observed to be lower than average. Over the north east (NE) the number of rainy days is still overestimated compared to observations.

The categorical verification scores for the UM Day1 forecasts over India are summarized using box and whisker plots in Figure 8. Scores are computed for each rainfall threshold based on all the observation/forecast pairs of each day during the six monsoon seasons and represent the grid scale QPF performance that may be expected on any given day. The verification results are presented against both TRMM and NSGM data.

The panels in the top row (Figure 8a,b) show the Probability of Detection (POD) and Success Ratio (SR). While POD indicates the fraction of observed 'yes' events forecast correctly, SR indicates the fraction of forecast 'yes' events that were actually observed. Both scores range from 0 to 1 with 1 being a perfect score. Both the scores have high values for rainfall thresholds below 20 mm d^{-1}. The verification of forecast against

the NSGM shows higher scores at all thresholds compared to verification against TRMM.

The two panels in the middle row (Figure 8c,d) show Probability of False Detection (POFD) and Bias Score or Frequency Bias (BIAS). POFD indicates what fraction of 'no' events were incorrectly forecast as 'yes' events. POFD varies from 0 to 1 with 0 being a perfect score. The POFD values indicate that forecasts have high false alarms at low rainfall thresholds. Again, the verification against the NSGM shows better score values compared to TRMM. The Frequency Bias (BIAS) indicates how the observed and forecast frequency of 'yes' events compare. BIAS varies from 0 to ∞ with 1 indicating a perfect forecast, BIAS>1 indicating over-forecasting and BIAS<1 indicating under-forecasting. The BIAS in Fig. 8 suggests the model is over-forecasting rain occurrence, particularly at lower thresholds (<20mm d^{-1}), consistent with Fig. 6.

Similarly, the panels in the bottom row (Figure 8e,f) show the box and whisker plots for two summary scores, the Equitable Threat Score (ETS) and Hanssen and Kuipers score (HK Score). While ETS tells how the forecast 'yes' events correspond to observed 'yes' events (accounting for random hits), HK Score tells how well the forecasts separate the 'yes' and 'no' events. For both scores, 0 denotes no skill and 1 means a perfect score. The ETS and HK show low values of the score at all rainfall thresholds. As before, relatively higher scores are obtained when the forecasts are verified against the NSGM.

3.2 Example of CRA Verification over India

The forecast errors are assessed in terms of displacement, pattern, and intensity using the CRA verification method. We first demonstrate the application of CRA verification and discuss the interpretation of the results. Figure 9 shows an example of CRA verification corresponding to a heavy rain event over western India on 3rd July 2007 associated with a low pressure system that formed over the Arabian Sea close to the Indian coast and moved inland over the Gujarat region. The verification scores indicate moderate skill (correlation=0.55; ETS=0.33; HK=0.61 and POD=0.82). The RMSE was 24.5 mm d^{-1}, about half of the observed mean rainfall. Although the forecast underestimated the average rain rate, the predicted rain volume was higher than the observations due to a larger area of rain being predicted. The biases can be related to high forecast rainfall along the Myanmar coast and along the foothills of Himalayas.

Figure 10 shows the CRA verification using a 10 mm d^{-1} threshold to isolate the heavy rainfall along the west coast of India. The CRA is bounded by the domain from 8.5° - 26°N and 69° – 78.5°E and includes 72 grid points. The scatter diagram shows the correspondence between the forecast and observed rainfall after attaining the best match (r_{OPT}) by shifting the forecast slightly to the north. For this forecast, the CRA verification shows a very modest improvement in correlation from 0.41 to 0.44. The error decomposition shows the primary contribution to the overall error came from the pattern error (86%).

3.3 CRA verification results for 2007-2012

The rainfall over different parts of India can be associated with different synoptic regimes as well as having different topography and proximity to neighbouring seas. The four regions shown in Figure 7 can be considered as rainfall zones for CRA verification. The rainfall over north-eastern India (NE) and the south-western peninsula (SW) strongly reflects the effects of the low level monsoon flow and the orographic enhancement over the mountains. The rainfall over eastern India (E) can be associated with the monsoon trough and south-easterly flow from the Bay of Bengal. The monsoon trough extends from north-western India to the head of the Bay of Bengal. The low pressure systems that develop over the Bay of Bengal and track in the westerly and north-westerly direction also significantly contribute to the rainfall over eastern India (E). Some of the low pressure systems track far inland in the westerly and north-westerly direction to produce rainfall spells over the arid and dry regions of northwest India (NW). However the rainfall over the NW region is some times associated with eastward passage of an upper-level trough/low in the mid-latitude westerlies and their interaction with the inland low pressure systems.

CRA verification results are presented for each zone based on the central location of the CRA. These results are based on the CRA statistics from six monsoon seasons (2007-2012) and for four different rainfall thresholds (10, 20, 40 and 80 mm d^{-1}). Table 2 shows the number of CRAs in each zone and for different CRA thresholds. Verification using the

TRMM analysis gives a slightly higher total number (940, 770 and 85) of CRAs (all four zones combined) compared to verification against the NSGM analysis (901, 541 and 51) for 10, 20 and 40 mm d^{-1} CRAs respectively. This is mainly reflected in three zones of NW, E and NE and can be attributed to the TRMM rainfall data estimating a greater frequency of heavy rain events (refer to Figure 6). However the total number of good matches is higher for CRA verification involving NSGM analyses (546, 217 and 18) compared to TRMM (381, 147 and 12). NSGM analyses are smoother and more conducive to higher correlations. For the 10 mm d^{-1} threshold, a good match is obtained in over 50% of the CRAs. The percentage of good matches decreases with the increasing CRA threshold indicating the decreasing skill of the NWP forecast model to predict the heavy rainfall. For an 80 mm d^{-1} CRA threshold (not shown) the number of good matches is so low that it does not form a good sample for analysis. The percentage of good matches for the 10 and 20 mm d^{-1} threshold is high (60% and 40%, respectively) for NSGM and relatively low (40% and 19%, respectively) for TRMM. The CRA verification results for these thresholds can be considered robust and significant, while for the 40 mm d^{-1} CRA threshold, the number of good matches is low (35% for NSGM and 14% for TRMM) and the results of the CRA verification should be viewed with caution.

Based on the good matches, the scatter plots in Figure 11 show the association among the observed and forecast average rainfall for rain systems located in each of the four zones. The difference in the CRA

verification results for TRMM and NSGM is rather striking in all zones and for all thresholds. Especially over the SW region, the model bias brought out in the NSGM (panels on right) is not seen as clearly in the TRMM (panels on left) which has fewer samples. Similarly, Figure 12 shows the association among the observed and forecast maximum rain in each of the four zones. The scatter of mean rain intensity (Figure 11) and maximum rain intensity (Figure 12) over NE India consistently suggest overestimation of rain intensity in the forecasts. Over the SW region, the forecasts tend to underestimate rain intensity. The nature of bias seen in the mean rain intensity (Figure 11) is also reflected in the maximum rain intensity (Figure 12). It is likely that the model forecasts tend to rain more over the ocean. In the present investigation, the verification is carried out over the land.

The average CRA verification statistics (after obtaining the best match of the forecast with the observations) using NSGM as observation data are compiled in Table 3. Figures 13 and 14 complement the information in Table 3. Figure 13 (left panel) shows the scatter of position errors (in degrees latitude and longitude) in each of the four zones in the Day1 forecasts. Each point in scatter plots shows the east-west versus north-south displacement in the centre of gravity (COG). Clustering of these points indicates increased frequency. Panels on the right show the spatial distribution of the counts of the position errors. The spatial distribution counts are not shown for 40 mm d^{-1} CRAs since the available points are too few. Similar distributions are evident in the Day3 and Day5

forecasts (not shown). Figure 14 shows the distributions of the position errors and post-correction spatial correlations using box-whisker plots.

The mean pattern correlation (and the RMSE in mm d^{-1}) achieved after correcting for location error are presented in Table 3. The pattern correlation (and RMSE) values range from 0.45 to 0.64 (18.3 to 30.7 mm d^{-1}) for lower CRA thresholds (10 and 20 mm d^{-1}). These can be considered robust since they are based on a large sample. For a higher CRA threshold (40 mm d^{-1}), the pattern correlation (0.49 to 0.68) and RMSE values (30 to 37 mm d^{-1}) are higher since the focus is on a smaller area of heavier rain, but due to the much smaller sample size these mean results contain greater uncertainty.

The mean displacement errors are given in degrees latitude and longitude in Table 3. *Positive* (*negative*) values of *x-displacement error* indicates that rain events are forecast to the *east* (*west*) of the observed location. Similarly, *positive* (*negative*) values of *y-displacement error* indicates that rain events are forecast to the *north* (*south*) of the observed location. The largest mean *x-displacement error* is in the eastern region (E) with forecasts located an average of 2° longitude eastwards for CRAs defined by the 10 mm d^{-1} threshold. This is consistent with the reported slow movement of the low pressure systems (Iyengar et al. 2011 and 2014) in model forecasts over eastern India after landfall. The magnitude of *x-displacement error* in eastern India (E) is seen to decrease for higher CRA thresholds. This clearly suggests that in eastern India (E), the location of heavier rain is predicted with greater accuracy

than the lighter rain events. The mean north-south displacement errors given by y-*displacement error* are relatively moderate with mean values less than 1° latitude.

The contributions to the total error due to displacement , volume and pattern are also summarized in Table 3. In all four regions, the contribution from pattern error forms the highest share for the 10 mm d^{-1} CRAs, which tend to have larger areas. Over E and SW regions, the relative contribution of pattern error (*displacement error*) decreases (*increases*) for 20 and 40 mm d^{-1} CRAs.

Referring to Figure 13, it can be noted that over the NW region, for 10 mm d^{-1} CRAs, the forecast location errors are spread in eastern quadrant with highest counts of 6 just east of the origin. Over the SW region, the scatter of the position errors (panels on left) shows a systematic southeast to northwest orientation typical of the rainfall along the west coast of India with a majority of forecasts displaced to the west of the observed event (also seen in Figure 14b). Over eastern India (E), the 10 mm d^{-1} CRAs tend to be forecast to the east of the observed location with a high count of 21 and 19 showing displacement by 1° east and south-eastwards respectively. Forecast rainfall in the NE region tends to be systematically predicted to the south of the observed location with high count of 17 at 1° south of observed location.

The vector errors are highest for 10 mm d^{-1} CRAs in all regions except over the NE region where the vector errors for 10 and 20 mm d^{-1} CRA thresholds are comparable. These are based on fewer samples

compared to the 10 and 20 mm d^{-1} CRA results, and represent stronger storms on average. Overall, vector errors were lowest in the SW, probably reflecting the strong orographic influence on the rainfall in that region.

The panels in Figure 15 show the RMSE (mm d^{-1}) and the percentage contribution to total error due to location, volume and pattern error. Not surprisingly, the RMSE is least for 10 mm d^{-1} CRAs with generally lower spread as this sample includes a larger proportion of lighter rainfall events. The 20 and 40 mm d^{-1} CRAs show higher RMSEs and greater variability. The contribution from pattern error is dominant in all four regions for 10 mm d^{-1} CRAs with the median value ranging from 60% in the NE region to 80% in the E region. The median contribution to error due to displacement is around 15% for all regions for 10 mm d^{-1} CRAs. This low relative contribution from displacement in the E region is surprising, given the large systematic eastward errors seen in Figures 13 and 14, but the pattern error in this region is very large and dominates the total error. Contributions from volume error are generally least except in the SW and NE regions where they are responsible for a similar proportion as the displacement errors.

4. Summary and Conclusions

The present study forms an important component of India's National Monsoon Mission (NMM) Programme to investigate and quantify the rainfall forecast biases in the Unified Model as part of an overall scientific challenge to better predict the Indian monsoon. This study has

examined the performance of the Met Office Unified Model (UM) over India for six years (2007-2012) during the monsoon season, using both TRMM 3B42 and the IMD blended gauge analysis (NSGM). Both data sets provide useful reference data for verification, though differences in the detection ability, spatial structure, and intensity distributions of TRMM and NSGM observed data sets lead to better performance of the model when compared to NSGM as opposed to TRMM (Figure 6, Table 2).

The model forecasts show a wet bias resulting from an excessive number of rainy days compared to observations all over India. In particular, the model has a higher frequency of rainfall occurrence at all thresholds from 0-20 mm d^{-1} compared to both sets of observations, while the forecast frequency of rain greater than 20 mm d^{-1} is well represented.

Systematic errors in the forecast rain systems are estimated using CRA analysis with 10, 20 and 40 mm d^{-1} threshold for four regions: the north-west (NW), south-west (SW), east (E) and north-east (NE). The mean and maximum rain amounts tended to be overestimated in the E and NE regions but underestimated in the mountainous SW region.

The displacement errors are scattered but show some systematic trends, depending on the CRA threshold. In the NW and SW, the forecast events are frequently displaced by about 1° to the north and 1° to the west, respectively, of the observed position. Over eastern India (E) forecasts for lighter rainfall events tend to be displaced about 1° to the east while heavier forecast rainfall events are displaced slightly southwest

of the observed location by about 1°. Southerly forecast displacements are most common in the NE region.

For 10 mm d^{-1} CRAs, the contribution from pattern error is dominant in all four regions, and the contribution from volume error is generally least. The relative contribution to total error due to displacement tends to increase with increasing CRA threshold as the relative contribution from pattern error decreases.

The information on the dominant contribution to the total error in any region may be useful guidance for the forecaster. For example, over the plains adjoining the Himalayas, it is often seen that the UM forecasts produce excess rainfall mainly associated with a prominent easterly bias in the 850 hPa winds (Iyengar et al. 2011). Another example is the rainfall associated with the Bay of Bengal low pressure systems where the predicted low pressure systems in the model make a rather slower than observed west north-westerly movement. The impact of position errors are reflected in Figures 13-15 for region E.

The detailed analysis presented in this study can help the model developers and forecasters to understand the systematic errors associated with forecast characteristics of monsoon rainfall over different parts of India. A similar analysis of QPFs from other modelling systems will provide robust measures of bias, accuracy, and relative error components in forecast rain systems over India. Additionally, plausible sources of forecast errors including grid resolution, model initialization, and physical processes will be addressed in future studies.

Acknowledgements The authors thank Noel Davidson of CAWCR and other colleagues in NCMRWF for fruitful interactions, scientific discussions in addition to comments/feedback that were useful in finalizing the manuscript. The model forecast data used in this study is obtained from the Met Office which is duly acknowledged. This work was supported by the Government of India, Ministry of Earth Sciences National Monsoon Mission under project MM/SERP/CAWCR-AUS/2013/INT-6/002.

References:

Ashrit R. and S. Mohandas 2010: Mesoscale model forecast verification during monsoon 2008. J. Earth Syst. Sci. 119, No. 4, 417–446

Bessafi, M. and M. C. Wheeler, 2006: Modulation of south Indian Ocean tropical cyclones by the Madden-Julian oscillation and convectively-coupled equatorial waves. Mon. Wea. Rev., 134, 638-656.

Brown, A.R., Beare, R.J., Edwards, J.M, Lock, A.P., Keogh, S.J., Milton, S.F., and Walters,D.N., 2007: Upgrades to the boundary layer scheme in the Met Office NWP model.Bound. Lay. Meteorol., **118**, 117-132.

Chen, Y., E.E. Ebert, K.J.E. Walsh, and N.E. Davidson, 2013: Evaluation of TRMM 3B42 daily precipitation estimates of tropical cyclone rainfall over Australia. *J. Geophys. Res.*, in revision.

Das S, Ashrit R, Gopal R Iyengar, Saji Mohandas, Das Gupta M, John P George, Rajagopal E N and Surya Kanti Dutta 2008: Skills of different mesoscale models over Indian region during monsoon season: Forecast errors.J. Earth Syst. Sci. 117(5) 603–620.

Davies, T.,M. J. P. Cullen, A. J. Malcom, M. H. Mawson, A. Staniforth, A. A. White and N. Wood 2005: A new dynamical core for the Met Office's global and regional modeling of the atmosphere, Q. J. R. Meteorol. Soc. (2005), 131, pp. 1759–1782.

Ebert, E.E. and J. L. McBride, 2000: Verification of precipitation in weather systems: Determination of systematic errors. J. Hydrol., 239, 179-202.

Ebert E.E., 2008: Fuzzy verification of high-resolution gridded forecasts; A review of proposed framework. Meteorol. Appl. 15, 51-64.

Ebert, E.E. and W. A. Gallus Jr, 2009: Towards better understanding of Contiguous Rain Areas (CRA) method of spatial verification, Weather and Forecasting, 24, 1401-1415

Edwards J.M. and A. Slingo, 1996: Studies with a flexible new radiation code Part I. Choosing aconfiguration for a large-scale model. Q. J. R. Met. Soc., **122**, 689-719.

Gilleland, E., D. A. Ahijevych, B. G. Brown and E. E. Ebert, 2010: Verifying forecasts spatially. Bull. Amer. Met. Soc., 1365-1373.

Goswami, B. N. and R. S. Ajaya Mohan, 2001: Intra-seasonal oscillations and inter-annual variability of the Indian summer monsoon. J. Climate, 14, 1180-1198.

Goswami, B. N., R. S. Ajaya Mohan, P. K. Xavier, and D. Sengupta, 2003: Clustering of low pressure systems during the Indian summer monsoon by intraseasonal oscillations. Geophys. Res. Lett., 30, 1431, doi:10.1029/ 2002GL016734.

Grams, J.S., W.A. Gallus, L.S. Wharton, S. Koch, A. Loughe, and E.E. Ebert, 2006: The use of a modified Ebert-McBride technique to evaluate mesoscale model QPF as a function of convective system morphology during IHOP 2002. *Weather and Forecasting*, **21,** 288–306*.*

Grant, A.L.M., 2001: Cloud base mass fluxes in the cumulus capped boundary layer*. Q. J. R. Met. Soc.* **127,** 407-421.

Gregory, D. and S. Allen, 1991: The effect of convective scale downdraughts upon NWP and Climate. *Proc. 9th AMS conf on NWP*, Denver, USA, 122-123.

Gregory, D. and P.R. Rowntree, 1990: A mass flux convection scheme with representation of cloud ensemble characteristics and stability-dependent closure. Mon. Wea. Rev., **118**,1483-1506.

Harper, K., L. W. Uccellini, E. Kalnay, K. Carey, and L. Morone, 2007: 50th anniversary of numerical weather prediction. Bull. Amer. Meteor. Soc., 88, 639–650.

Iyengar, G., R. Ashrit, M. Das Gupta, and co-authors, 2011: NCMRWF & UKMO Global Model forecast verification: Monsoon 2010. Monsoon Report, NMRF/MR/02/2011.

Iyengar, G. R., Raghavendra Ashrit, Kuldeep Sharma and E.N. Rajagopal 2014: Monsoon-2013: Performance of NCMRWF Global Assimilation-Forecast System, Monsoon Report, NMRF/MR/01/2014.

Jolliffe, I.T. and Stephenson, D.B., 2011: Introduction, in Forecast Verification: A Practitioner's Guide in Atmospheric Science, Second Edition (eds I. T. Jolliffe and D. B. Stephenson), John Wiley & Sons, Ltd, Chichester, UK. doi: 10.1002/9781119960003.ch1

Kalnay, E., S. J. Lord, and R. D. McPherson, 1998: Maturity of operational numerical weather prediction: Medium range. Bull. Amer. Meteor. Soc., 79, 2753–2769.

Maloney, E. D. and D. L. Hartmann, 2000: Modulation of eastern North Pacific hurricanes by the Madden-Julian oscillation. J. Climate, 13, 1451-1460.

Mandal, V., U.K. De and B.K. Basu 2007: Precipitation forecast verification of Indian summer monsoon with intercomparison of the three diverse regions. Weather and Forecasting, 22, 428-443.

Mitra A. K., A. K. Bohra, M. N. Rajeevan, T. N. Krishnamurti, 2009: Daily Indian precipitation analysis formed from a merge of rain gauge data with TRMM TMPA satellite-derived rainfall estimates. J. Meteor. Soc. Japan, 87A, 265-279.

Prakash, S., V. Satyamoorthy, C. Mahesh and R. M. Gairola 2014: An evaluation of high-resolution multisatellite rainfall products over the Indian monsoon region. Int. J. Remote Sensing, 35(9), 3018-3035.

Rawlins F, S. P. Ballard, K.J. Bovis, A. M. Clayton, D. Li, G.W. Inverarity, A.C. Lorenc and T.J.Payne, 2007: The Met Office global four-dimensional variational data assimilation scheme, Q. J. R. Met. Soc., **133**, 347–362

Simmons, A.J., and A. Hollingsworth, 2002: Some aspects of the improvement in skill of numerical weather prediction. Quart. J. Roy. Meteor. Soc., 128, 647–677.

Stephenson D.B., B. Casati, C.A.T. Ferro and C.A. Wilson, 2008: The extreme dependency score: a non-vanishing measure for forecasts of rare events. *Meteorol. Appl.*, **15**, 41-50.

Webster S., A.R. Brown, D. Cameron and C.P.Jones, 2003: Improvements to therepresentation of orography in the Met Office Unified Model. Q. J. R. Met. Soc., 126, 1989-2010

Wilks, D. S., 2011: Statistical Methods in the Atmospheric Sciences. International Geophysical Series Vol. 100., Academic Press.

Table 1. Some of the important Unified Model (UM) changes in recent years.

	UM Versions	**Configuration**
2007	UM6.4 (Feb2007), UM6.5 (Jul2007)	N320L50 (~40km in mid-latitudes)
2008	UM7.0 (Mar2008), UM7.1 (Aug2008)	N320L50 (~40km in mid-latitudes)
2009	UM7.3 (Mar2009), UM7.4 (Aug2009)	N320L70 (~40km in mid-latitudes) 12 min timestep
2010	UM7.6 (Apr2010), UM7.1 (Aug2010)	N512L70 (~25 km in mid-latitudes) 10 min time step 4DVAR data assimilation
2011	UM7.9 (Apr2011), UM8.0 (Aug2011)	N512L70 (~25 km in mid-latitudes) 10 min time step Hybrid data assimilation
2012	UM8.2 (Apr2012)	N512L70 (~25 km in mid-latitudes) 10 min time step Hybrid data assimilation

Table 2. The number of CRAs verified in each zone and the number of good matches.

CRA thresholds	Region	NSGM Total CRAs	NSGM Good matches	TRMM Total CRAs	TRMM Good matches
10mm	**NW**	93	55	90	42
	SW	280	183	154	57
	E	336	227	466	210
	NE	192	81	230	72
Total		**901**	**546**	**940**	**381**
20mm	**NW**	70	21	122	30
	SW	170	83	115	19
	E	210	84	302	63
	NE	91	29	231	35
Total		**541**	**217**	**770**	**147**
40mm	**NW**	5	1	12	1
	SW	23	9	12	1
	E	20	6	43	6
	NE	3	2	18	4
Total		**51**	**18**	**85**	**12**

Table 3. (a) Verification of Day1 rainfall forecasts (b) mean displacement errors and (c) components of total mean squared error (MSE) over four rainfall zones and for three CRA thresholds, as verified against NSGM data.

	10 mm d^{-1} threshold				20 mm d^{-1} threshold				40 mm d^{-1} threshold			
	NW	**SW**	**E**	**NE**	**NW**	**SW**	**E**	**NE**	**NW**	**SW**	**E**	**NE**
(a) Forecast Verification												
Pattern Correlation	0.54	0.63	0.45	0.48	0.58	0.64	0.55	0.48	--	0.59	0.68	-
RMSE(mm d^{-1})	18.3	21.1	18.8	18.6	30.1	30.7	23.5	30.0	-	41.0	30.0	-
(b) Displacement error (degrees)												
x-displacement (deg lon)	1.73	0.28	2.11	0.44	0.87	-0.15	0.75	0.29	-	0.13	0.51	-
y-displacement (deg lat)	0.82	0.58	0.44	-0.62	0.03	0.06	0.26	-0.19	-	-0.51	1.03	-
(c)% of total error due to												
Displacement error	19	19	17	20	26	17	29	23	-	20	60	-
Volume error	12	17	9	21	19	28	9	15	-	30	5	-
Pattern error	69	64	74	59	55	55	62	62	-	50	35	-

Figure Captions

Figure 1. Geographical domain over India used for rainfall verification showing terrain elevation (km) and typical distribution of the rain gauge network on any day during the monsoon season.

Figure 2. 24 hour rainfall valid for 22nd Aug 2012 in (a) TRMM (valid for 00UTC) and (b) NSGM (valid for 03UTC).

Figure 3. Frequency distribution of observed daily rainfall (JJAS) over India during 2007-2012. The box-whiskers compare the rainfall based on satellite estimates (TRMM) and satellite+gauge merged (NSGM). The comparison is presented for different rainfall thresholds. The values greater (lower) than 3/2 times the 75th percentile (25th percentile) are outliers.

Figure 4. CRA formed by overlap of forecast and observations.

Figure 5. (a) Observed (NSGM) and UM forecast (b)Day1, (c)Day2, (d)Day3 and (e)Day5 mean JJAS rainfall (mm d^{-1}) over India during 2012.

Figure 6. Observed and UM Day1 forecast rainfall frequency distribution over India.

Figure 7. (a) Observed (NSGM) and (b) UM Day1 forecast number of rainy (>1mm d^{-1}) days during JJAS 2012;(c)same as (b) with >2mm d^{-1}as the definition of a rainy day and (d) same as (b) with >5mm d^{-1}as the definition of a rainy day. The boxes show the four domains that are used to investigate regional variation in forecast performance.

Figure 8. Rainfall forecast verification scores for Day1 forecasts verified against TRMM 3B42 and NSGM rainfall analyses: (a) Probability of Detection (POD), (b) Success Ratio (SR), (c) Probability of False Detection (POFD), (d) Frequency Bias or Bias Score (BIAS), (e) Equitable Threat Score (ETS), and (f) Hanssen and Kuipers score (HK score).

Figure 9. Verification of forecast (left) rainfall over India valid for 3rd July 2007. Observed (NSGM; right) rainfall and the skill scores (using raining (>1mm) grids) are also shown.

Figure 10. CRA verification results for forecast rainfall along the west coast of India valid for 3rd July 2007. The CRA is defined using a 10mm d^{-1} threshold.

Figure 11. Forecast vs observed (TRMM, *left*; NSGM, *right*) mean rain intensity over four regions of India (NE,SW, E and NE) for three different CRA thresholds.

Figure 12. As in Figure 11 for maximum rain intensity.

Figure 13. Spatial distributions (scatter plots on *left*) of displacement errors and the CRA counts (shaded grids on *right*) in 1 degree grid box for individual rainfall zones and CRA thresholds. The x- and y- axes are in degrees longitude and latitude respectively**.(**computations are based on NSGM data**)**

Figure 14. Box-whisker plots summarizing the correlation, x-, y-, and vector errors (degrees) over (a) north west (NW) (b) south west (SW) (c) east (E) and (d) north east (NE).(Computations are based on NSGM data).

Figure 15. Box-whisker plots summarizing the RMSE and contribution to total error from displacement error, volume error and pattern error over (a) north west (NW) (b) south west (SW) (c) east (E) and (d) north east (NE).(Computations are based on NSGM data)

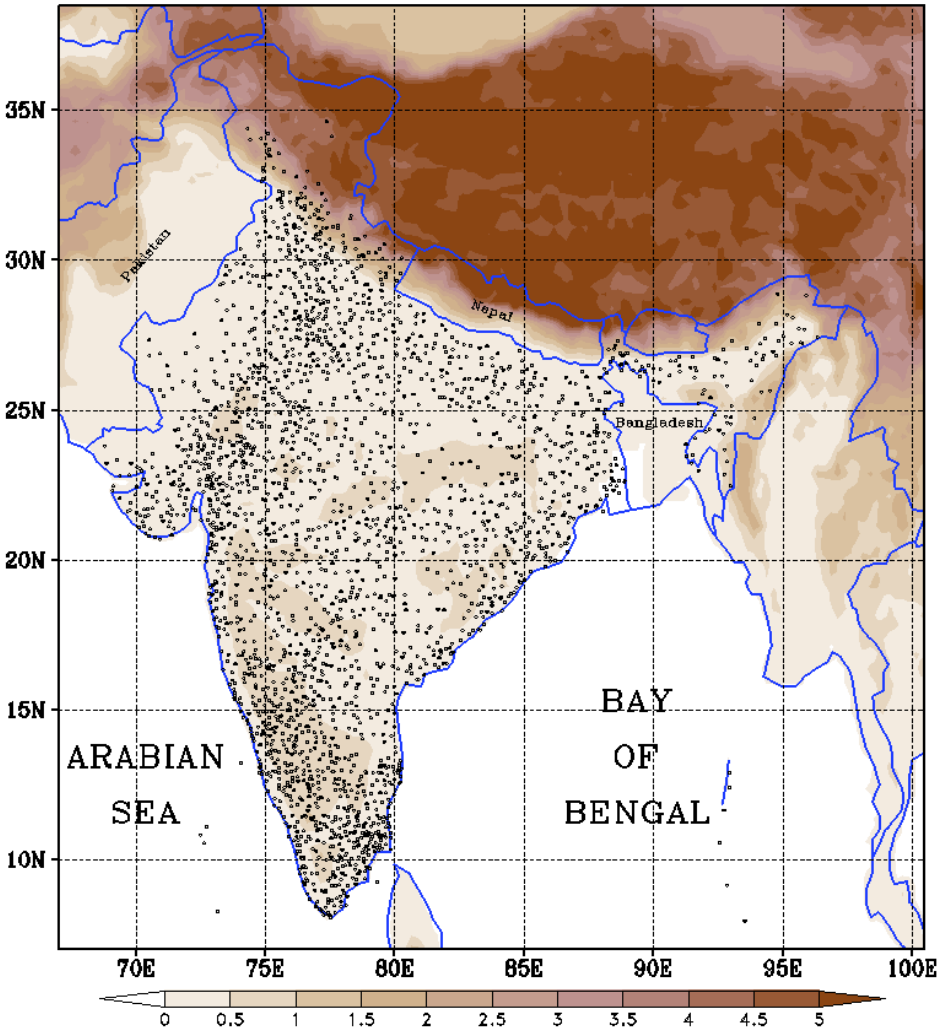

Figure 1. Geographical domain over India used for rainfall verification showing terrain elevation (km) and typical distribution of the rain gauge network on any day during the monsoon season.

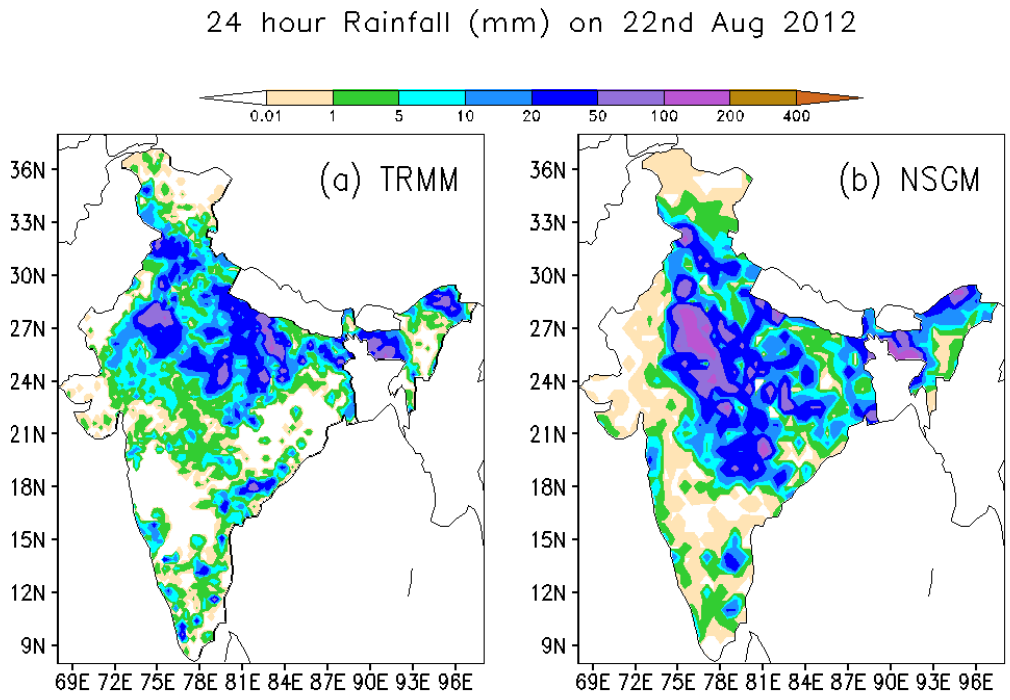

Figure 2. 24 hour rainfall valid for 22nd Aug 2012 in (a) TRMM and (b) NSGM. (TRMM rainfall is accumulated at 00UTC while NSGM rainfall is accumulated at 03UTC)

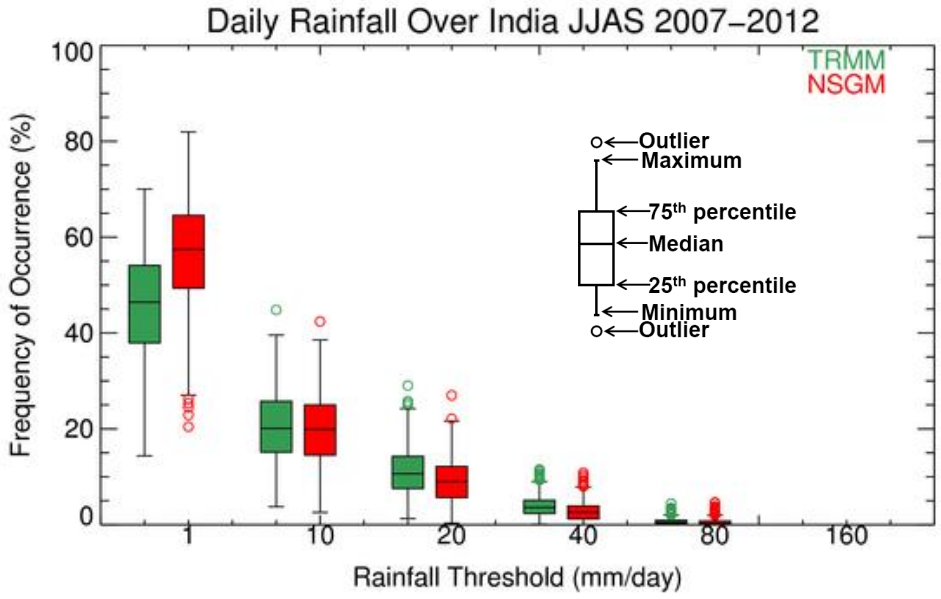

Figure 3. Frequency distribution of observed daily rainfall (JJAS) over India during 2007-2012. The box-whiskers compare the rainfall based on satellite estimates (TRMM) and satellite+gauge merged (NSGM). The comparison is presented for different rainfall thresholds. The values greater (lower) than 3/2 times the 75th percentile (25th percentile) are outliers.

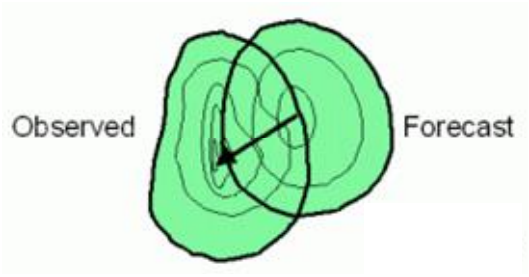

Figure 4. CRA formed by overlap of forecast and observations.

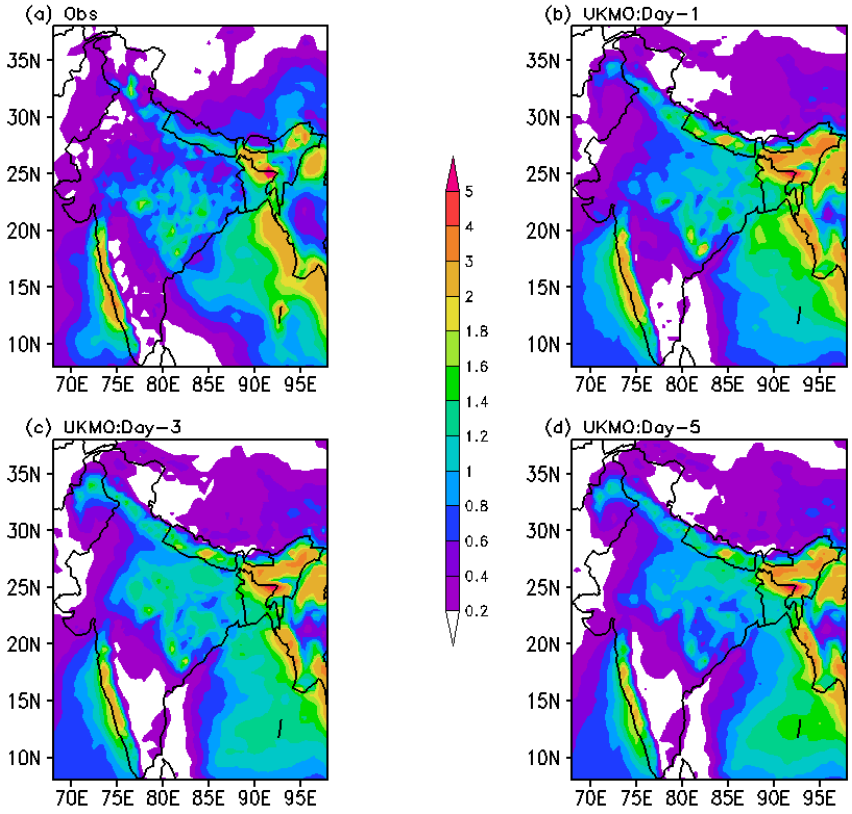

Figure 5. Observed (upper left) and forecast (Day1, Day3 and Day5) mean JJAS rainfall (mm/day) over India during 2012.

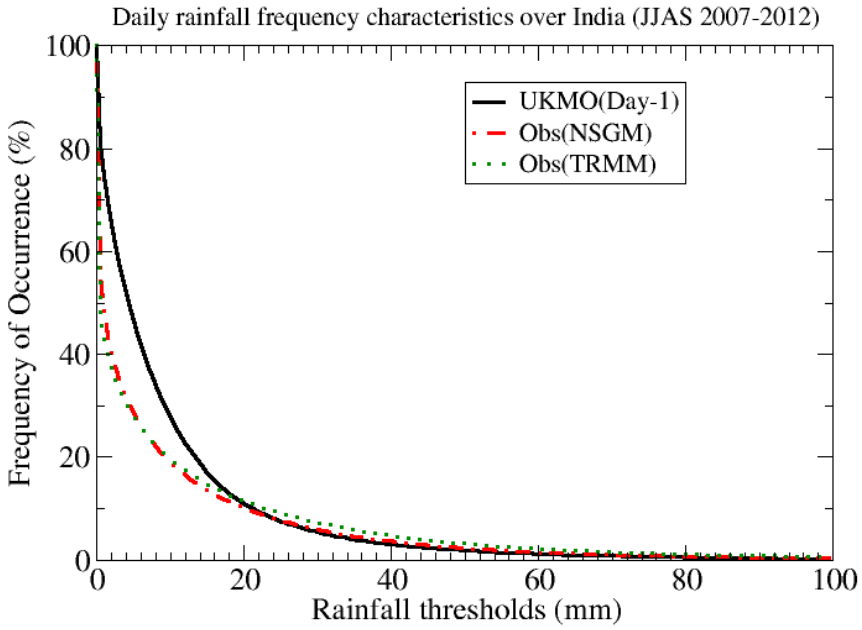

Figure 6. Observed and UKMO Day1 forecast rainfall frequency distribution over India.

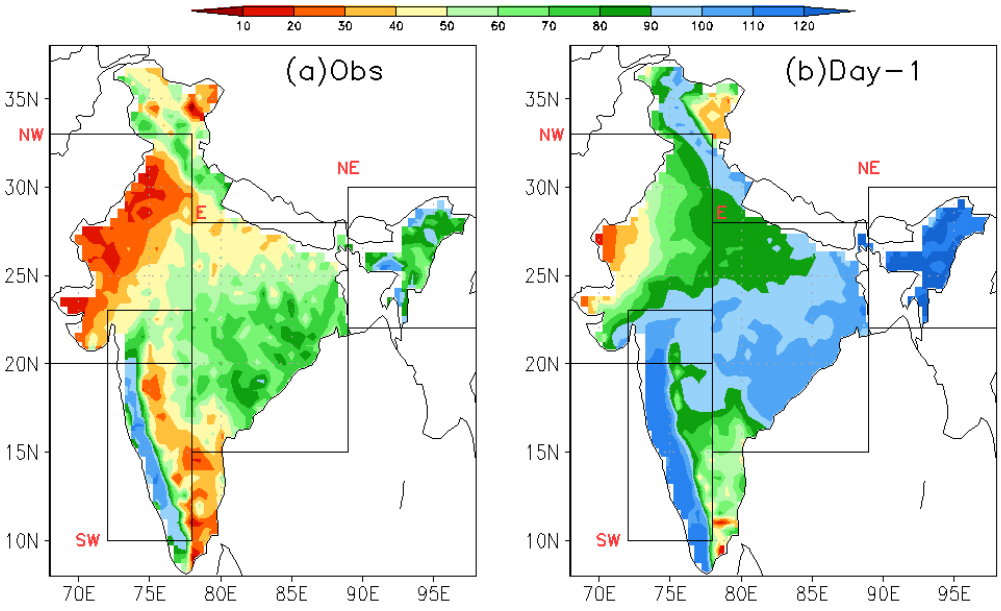

Figure 7. Observed (NSGM) and UKMO Day1 forecast number of rainy days (rainfall > 1mm/day) during JJAS 2012. The boxes show four domains that are used to investigate regional variation in forecast performance.

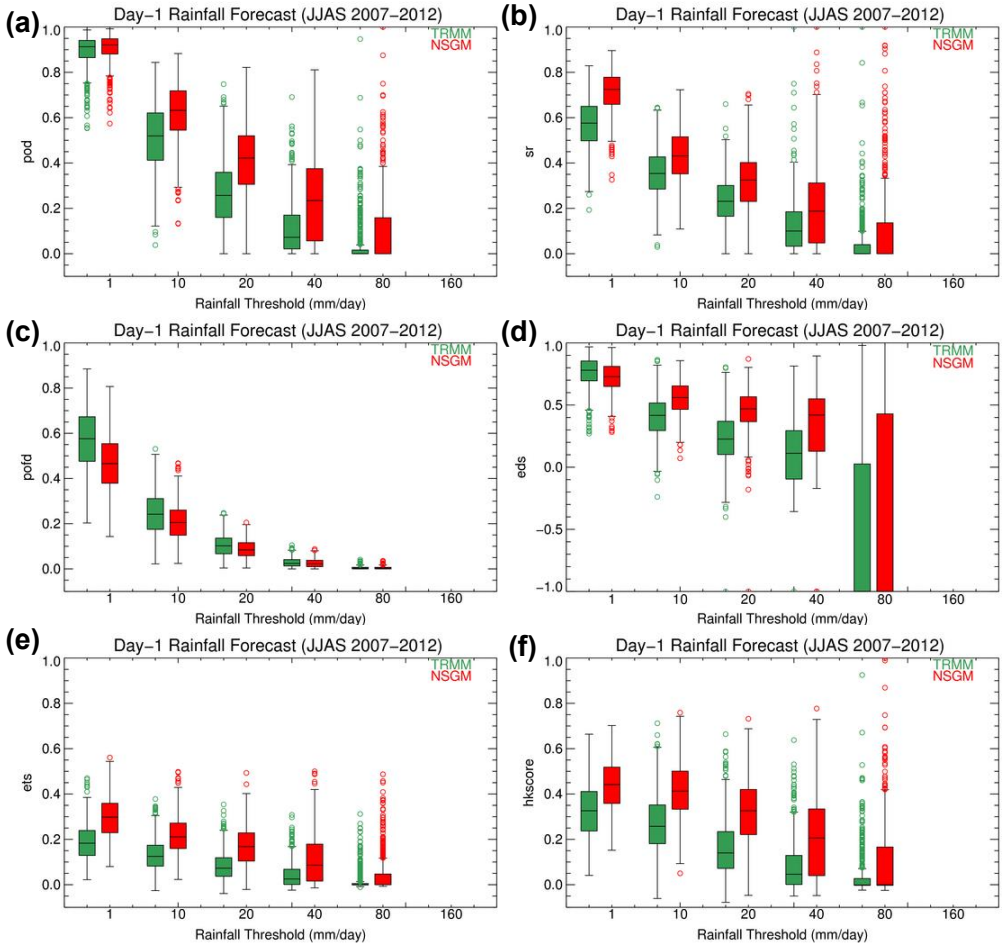

Figure 8. Rainfall forecast verification scores for Day1 forecasts verified against TRMM 3B42 and NSGM rainfall analyses: (a) probability of detection (POD), (b) success ratio (SR), (c) probability of false detection (POFD), (d) extreme dependency score (EDS), (e) equitable threat score (ETS), and (f) Hanssen and Kuipers score (HK score).

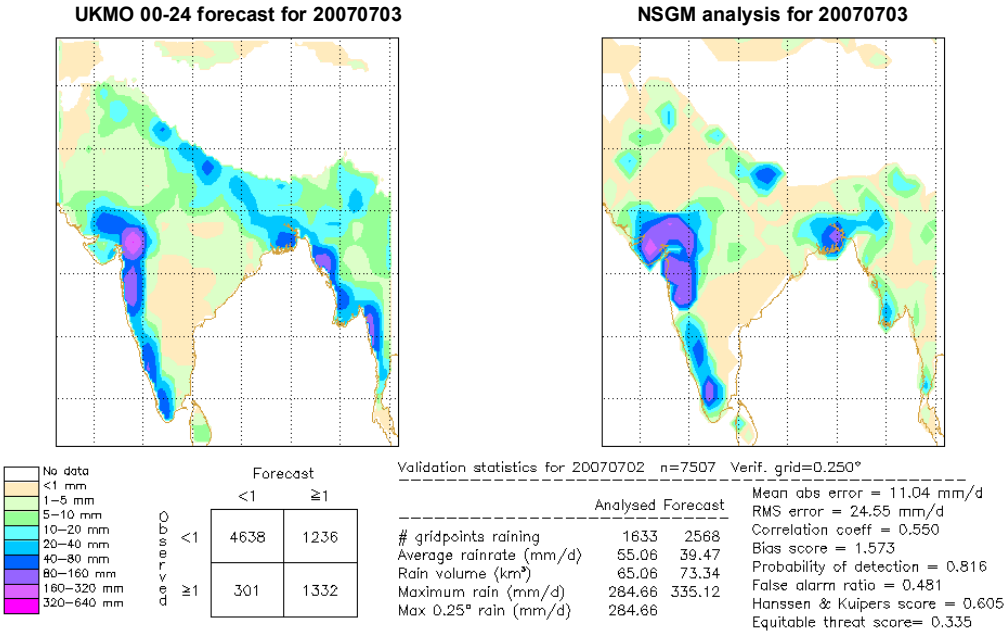

Figure 9. Verification of forecast (left) rainfall over India valid for 3rd July 2007. Observed (NSGM; right) rainfall and the skill scores are also shown.

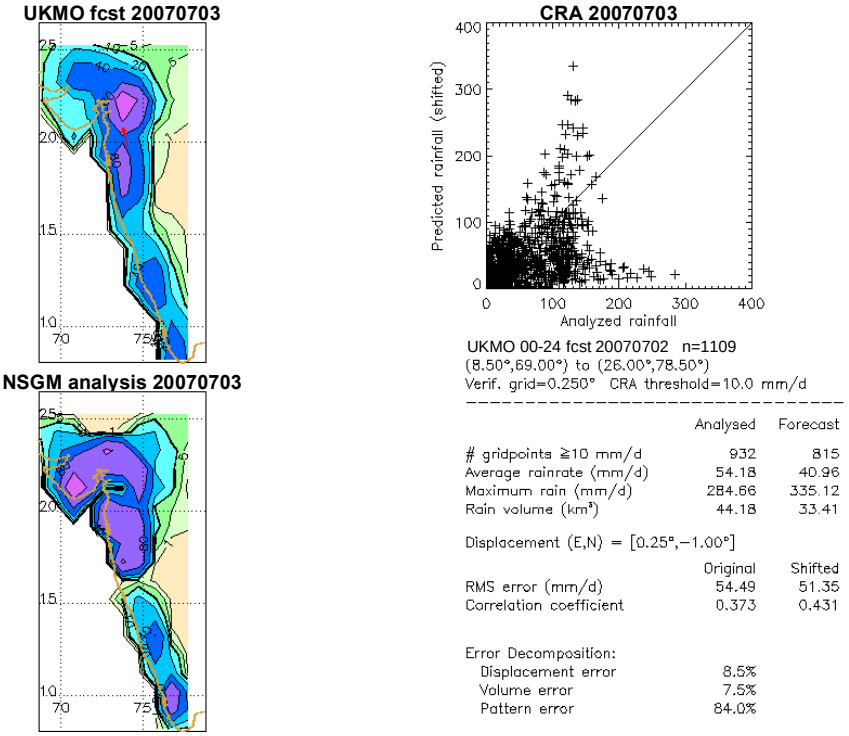

Figure 10. CRA verification results for forecast rainfall along the west coast of India valid for 3rd July 2007. The CRA is defined using a 10mm d^{-1} threshold.

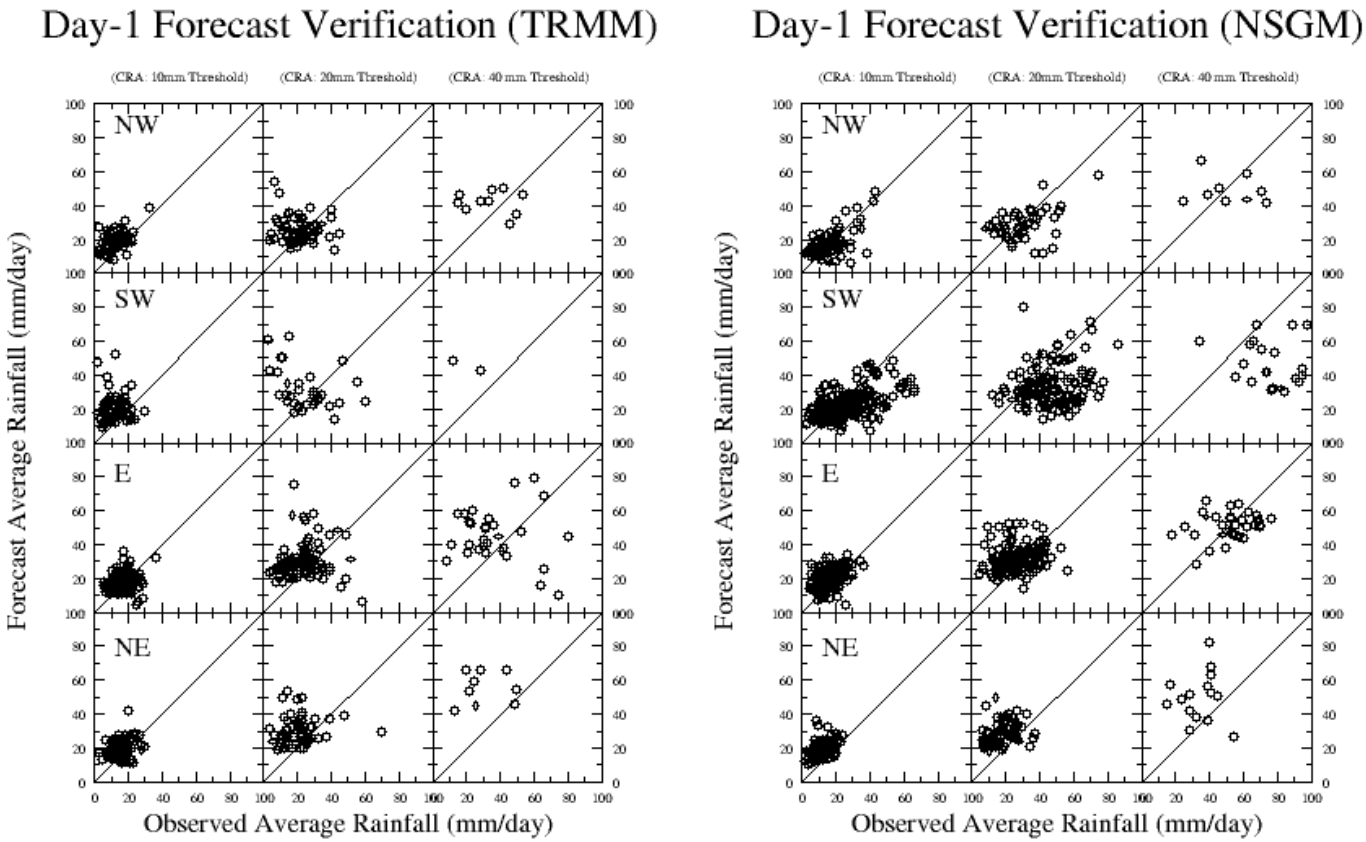

Figure 11. Forecast vs observed (TRMM, *left*; NSGM, *right*) mean rain intensity over four regions of India (NE,SW, E and NE) for three different CRA thresholds.

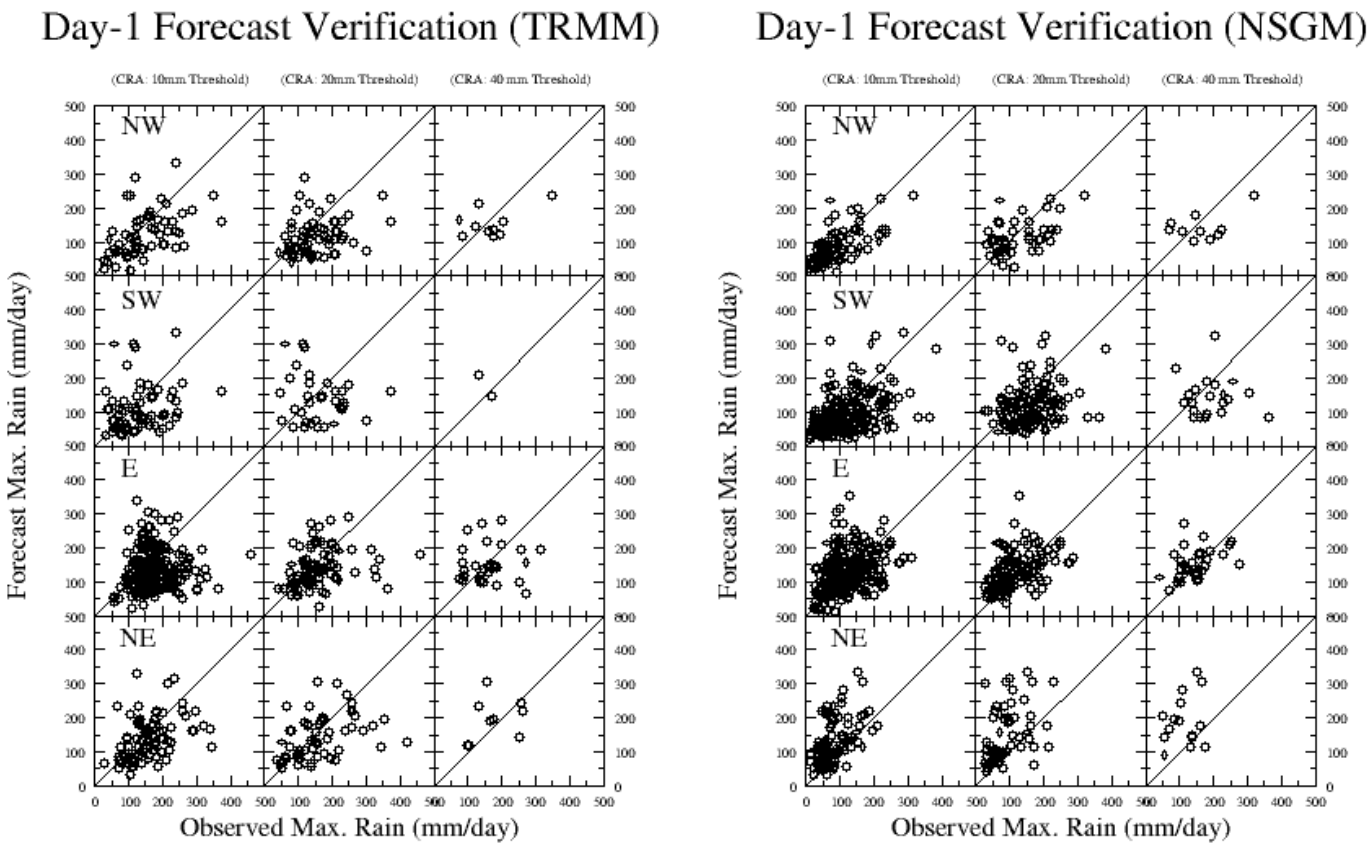

Figure 12. As in Figure 11 for maximum rain intensity.

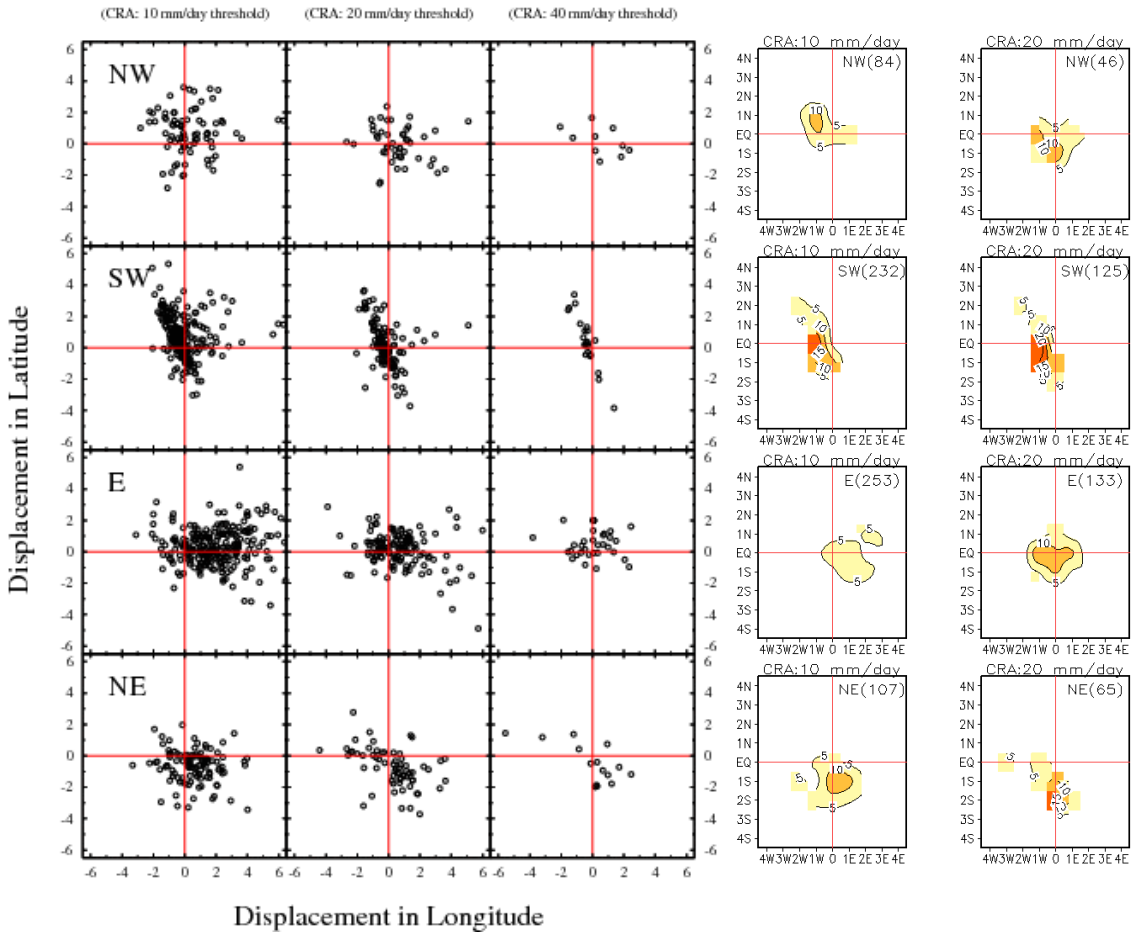

Figure 13. Spatial distributions (scatter plots on *left*) and frequency (shaded contour plots on *right*) of CRA displacements for individual rainfall zones and CRA thresholds. The x- and y- axes are in degrees longitude and latitude respectively.

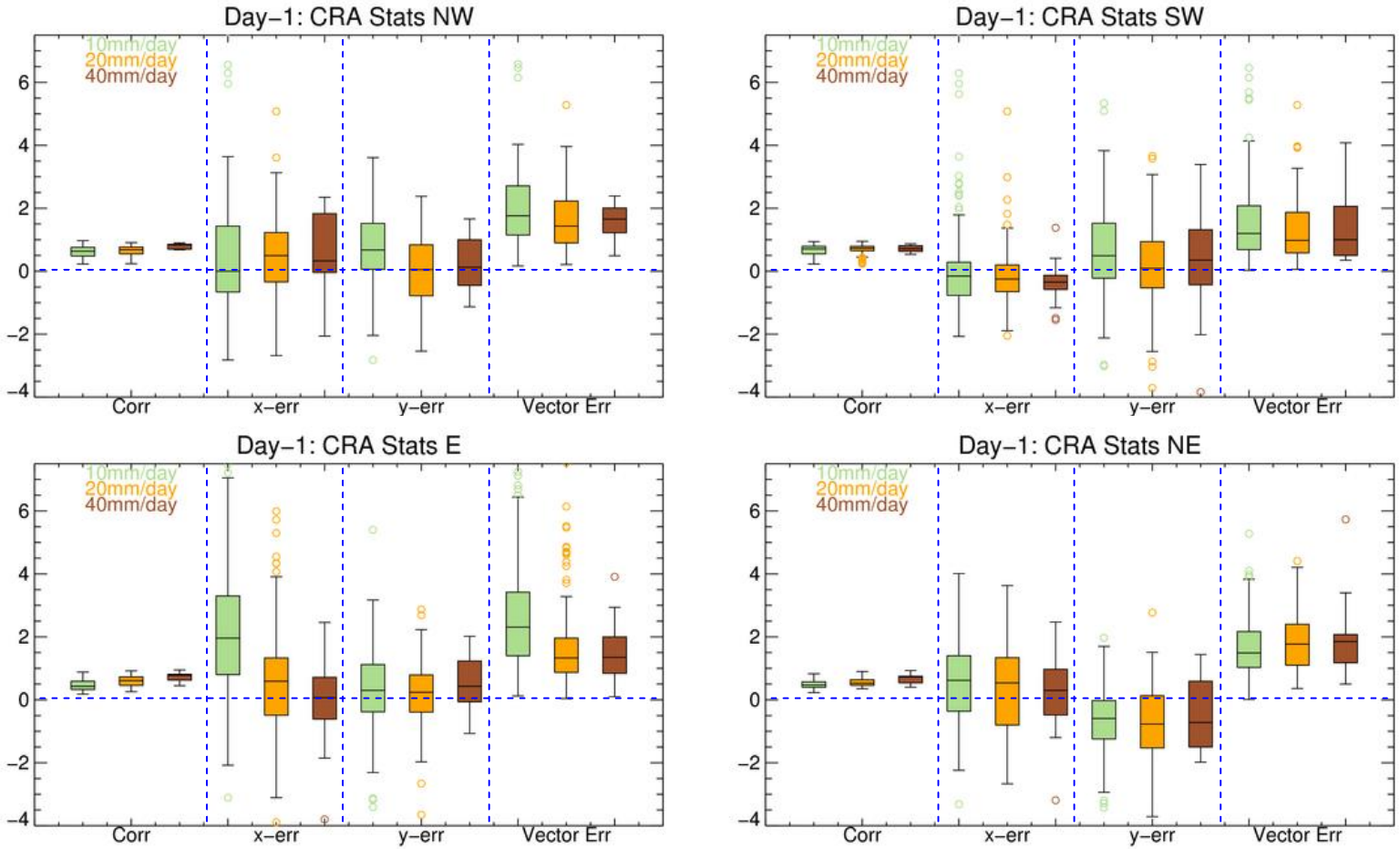

Figure 14. Box-whisker plots summarizing the correlation, x-, y-, and vector errors (degrees) over four rain zones.

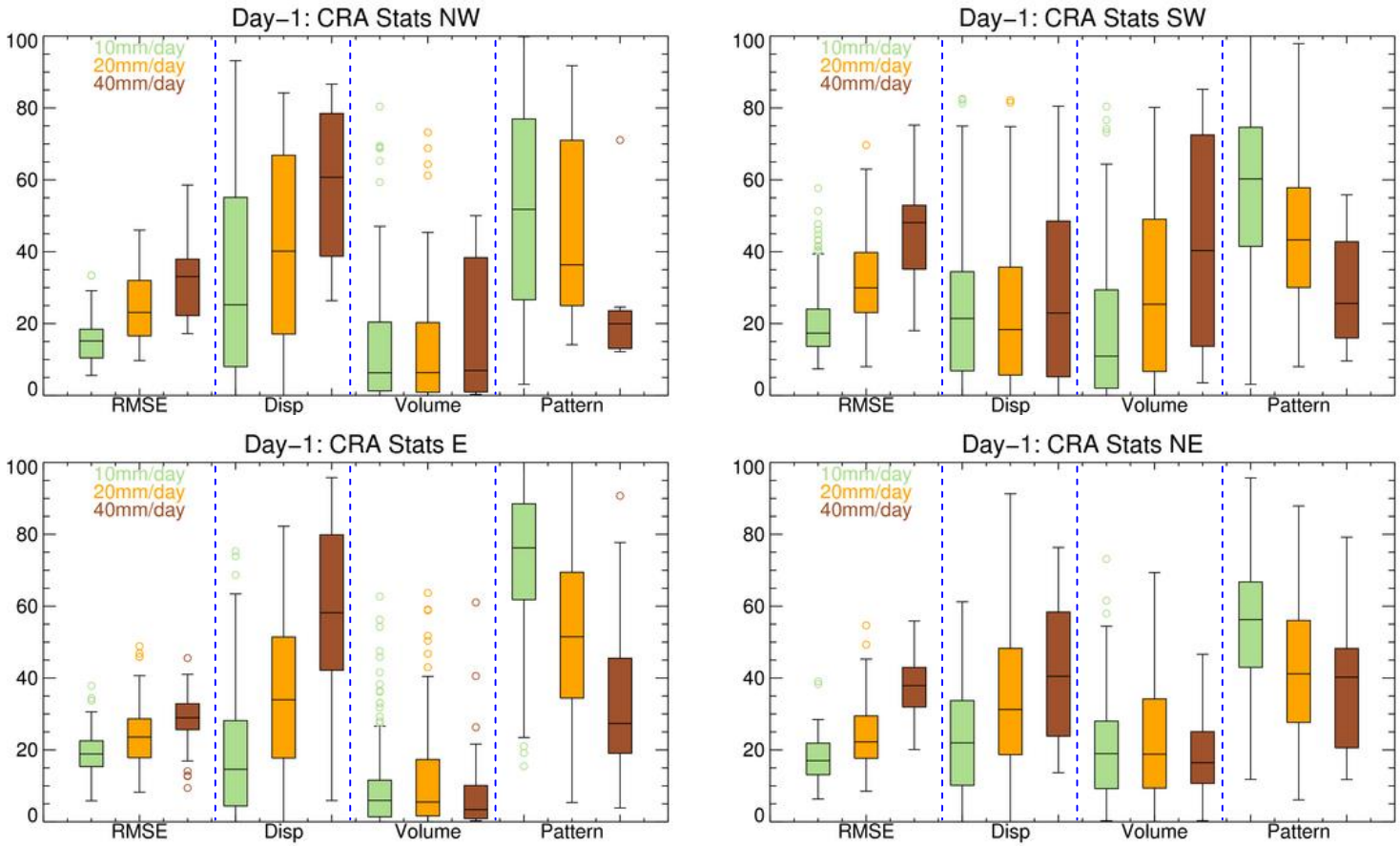

Figure 15. Box-whisker plots summarizing the RMSE and contribution to total error from displacement error, volume error and pattern error over four rain zones.